An aerodynamic study on flexed blades for VAWT applications

Daniel Micallef, Russell Farrugia, Tonio Sant, Pierluigi Mollicone

University of Malta, Faculty of Engineering, Department of Mechanical Engineering, Msida, MSD2080, Malta.

E-mail: `daniel.micallef@um.edu.mt`

Abstract. There is renewed interest in aerodynamics research of VAWT rotors. Lift type, Darrieus designs sometimes use flexed blades to have an 'egg-beater shape' with an optimum Troposkien geometry to minimize the structural stress on the blades. While straight bladed VAWTs have been investigated in depth through both measurements and numerical modelling, the aerodynamics of flexed blades has not been researched with the same level of detail.

Two major effects may have a substantial impact on blade performance. First, flexing at the equator causes relatively strong trailing vorticity to be released. Secondly, the blade performance at each station along the blade is influenced by self-induced velocities due to bound vorticity. The latter is not present in a straight bladed configuration. The aim of this research is to investigate these effects in relation to an innovative 4kW wind turbine concept being developed in collaboration with industry known as a self-adjusting VAWT (or SATVAWT). The approach used in this study is based on experimental and numerical work. A lifting line free-wake vortex model was developed. Wind tunnel power and hot-wire velocity measurements were performed on a scaled down, 60cm high, three bladed model in a closed wind tunnel.

Results show a substantial axial wake induction at the equator resulting in a lower power generation at this position. This induction increases with increasing degree of flexure. The self-induced velocities caused by blade bound vorticity at a particular station was found to be relatively small.

1. Introduction
Darrieus rotors (lift type) can use flexed blades with an optimum geometry based upon a Troposkien shape in order to reduce the structural stress in the blades. Depending on the structural design, due to centrifugal stresses, there can be a marked flexural effect resulting in aerodynamic effects that can be relatively complex. While straight bladed VAWTs have been investigated in depth through both measurements and numerical modelling, the aerodynamics of flexed blades is still somewhat obscure.

1.1. Current state of the art
There has been renewed interest in the application of VAWTs particularly in the built environment. Recent research work (see Scheurich & Brown [9]) has investigated the effects of unsteady wind conditions, as found in such environments, on blades having different geometries. Also in Kinzel et al. [8] a study of the flow over an array of VAWTs is given.

A review of the aerodynamics of Darrieus VAWTs having straight blades can be found in Islam et al. [6]. The review focuses on numerical modelling of the VAWT and the authors suggest

that vortex methods are suitable for application to a straight blade Darrieus VAWT rotor. While this statement is also also supported by work done on Horizontal-Axis wind turbines such as by Haans et al. [4], the applicability of such models to Darrieus type turbines having non-straight blades remains debatable due to complex phenomena such as blade-wake interactions and flow separation.

Ferreira et al. [2] use a 3D unsteady potential-flow vortex model to study the flow three-dimensionality of a straight bladed Darrieus VAWT. The dynamic stall phenomenon has been given particular attention also by Ferreira et al. [10] using Stereo Particle Image Velocimetry (SPIV) and more recently by Wang et al. using a 2D Navier Stokes approach. The work by Ferreira et al. [2] certainly confirms that the 3D vortex panel approach is generally speaking suitable for applications to VAWTs.

The aerodynamic loading response has been investigated for a curved blade Darrieus VAWT by El-Sayed et al. [1]. No details are mentioned of the aerodynamic effects of blade curvature and of the three-dimensional flow characterizing the VAWT. This is indeed a shortcoming of the current state of the art.

Various CFD simulations were performed in 2D and 3D have been performed such as by Kinzel et al. [3]but are again limited to straight bladed VAWTs.

In this work, the lack of insight on the effects of curved VAWT blades is addressed from a wake vorticity and mutual bound vorticity point of view.

1.2. Aims of the SATVAWT

A new VAWT concept has been proposed by industry based on the Darrieus flexed blade design. The innovative aspect of the design is that the blade geometry changes due to the centrifugal forces at high rotational speeds with the aim of facilitating start-up as well as mitigating structural stresses at high wind speeds. The new concept is called Self-Adjusting Vertical Axis Wind Turbine (SATVAWT). The driving idea behind the SATVAWT is to address the current major disadvantages of standard Darrieus type turbines.

In particular, the cut-in wind speed of this turbine is intended to be low by having a rotor of a low moment of inertia in its extended position (see Figure 1). At high wind speeds, the flexibility of the turbine blades allow for a larger equatorial radius and hence a larger moment of inertia about its rotating axis. A larger torque would be produced in this manner but the aerodynamic efficiency of such a configuration still needs further scrutiny. These two aspects provide fundamental advantages over the standard Darrieus machine.

1.3. SATVAWT: Rotor and blade geometry

The SATVAWT is a three-bladed rotor having geometries as shown in Figure 1 and 2 for the extended (low wind speed) and flexed (high wind speed) condition respectively. The height of the turbine is 3.8m while the equatorial radius is 1.2m. The turbine uses 3 blades with a constant chord of 0.3m and a blade twist and pitch of 0°. The SATVAWT blade uses a NACA0018 with the aim of reducing manufacturing costs of the blade due to the symmetric profile.

2. Experiment description

A 1:6.7 scaled down rigid model of the extended SATVAWT (see Figure 1) was built for experimental testing in a 0.9m diameter open return wind tunnel. the model was placed horizontally to facilitate the assembly of the turbine in the tunnel. A 100W motor was used to drive the turbine to a maximum speed of 1000RPM. The tunnel blockage factor (ratio of turbine projected area to tunnel area) was 20%. The Reynolds number range between $21,000 < Re < 57,000$. Both power and velocity measurements were carried out. A photograph of the rotating turbine is shown in Figure 3.
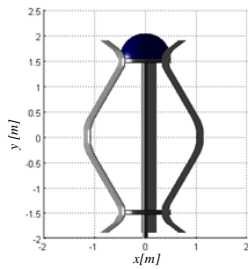
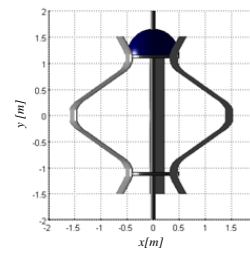**Figure 1.** Extended turbine geometry.

Figure 2. Flexed turbine geometry.

A torque meter was connected in series with the motor in order to measure the torque output from the turbine. This was then used to obtain the aerodynamic power output. A single probe hot wire anemometer was used in order to measure the three-dimensional velocity components using three different orientations. Reference is here made to Bruun [5] for a description of converting the raw data into velocities. The measurement points are shown in Figures 4 and 5 respectively. Measurements are taken from the vicinity of the tunnel wall to the turbine equator in order to take advantage of symmetry. In order to ensure a more accurate calculation of the mean velocity, 600 data samples are taken per point for every 1° blade azimuth.
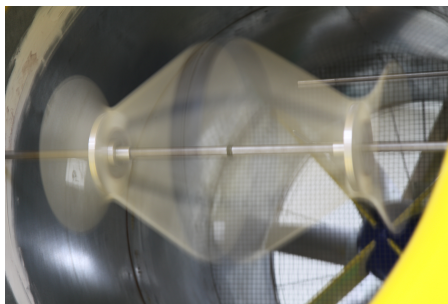

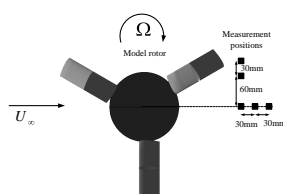**Figure 3.** Rotor rotating during experimental measurements.

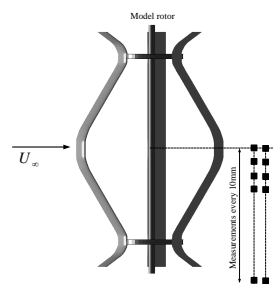**Figure 4.** Measurement locations along the horizontal and vertical planes.

Figure 5. Measurement positions along the blade.

3. Potential-flow vortex model
The potential-flow vortex model is based on the formulation by Katz and Plotkin [7] and van Garrel [11]. Both the blades and the wake are modelled using vortex filaments. The wake vortex

filaments arise due to spanwise and temporal variations in bound vorticity on the blade lifting line. These are called respectively trailing and shed vorticity. For a bound vorticity variation $\Gamma_B(r,t)$, the vorticity strength of trailing vortex filaments is given by:

$$\gamma_T = \frac{\partial \Gamma_B(r,t)}{\partial r} \tag{1}$$

$$\gamma_S = \frac{\partial \Gamma_B(r,t)}{\partial t} \tag{2}$$

where r = blade radial distance from the axis of rotation and t = time. The blade lifting line and the wake vortex filaments are depicted in Figure 6. The shed vorticity strength is given by:
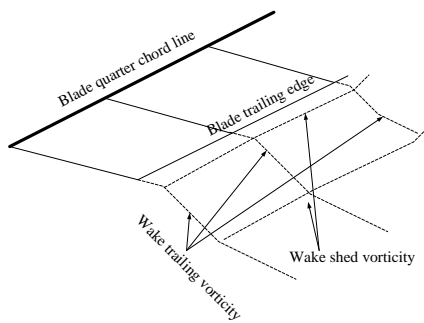

Figure 6. Vortex line representation of the blade and the released wake from the trailing edge.

The velocity induced by each vortex filament at a position vector $\vec{x_p}$ can be found by means of the Biot-Savart law:

$$\vec{V}(\vec{x_p}) = \frac{-1}{4\pi} \int \Gamma \frac{\vec{x} \times \vec{dl}}{x^3} \tag{3}$$

where $\vec{V}(\vec{x_p})$ is velocity induced at a point x_p, Γ is the vortex filament vorticity strength and $\vec{x}$ is the relative position vector of the vortex filament. The following algorithm is used for the numerical model:

(i) An initial seed of blade bound vorticity is applied

(ii) The velocity at each blade control point (at the blade lifting line is calculated)

(iii) The angle of attack may be found and hence the lift coefficient is found using the 2D polars

(iv) Estimate a new value of blade bound vorticity

(v) Check whether results converge to a specified tolerance

(vi) Once converged, release from the trailing edge, newly generated wake filaments

(vii) Calculate the induced velocity at each wake point and find a displacement using a first order Euler approach; $\vec{x_{new}} = \vec{V} * \Delta t$ where Δt is the time-step used in the simulation.

(viii) Repeat from step 2 onwards until all time steps are complete

No dynamic stall modelling was applied to the 2D input aerofoil data. Dynamic stall could have important implications on both loading and on the resulting flow.

Simulations were carried using the input parameters shown in Table 1. Simulations were carried out for the experimental model turbine at $U_\infty = 5.5 m/s$ and $\Omega = 1000 RPM$ and for the full scale turbine (both extended and flexed) at U_∞ = 6m/s, 8m/s, 12m/s and 45m/s with $\Omega = 220 RPM$.

Table 1. Major input parameters in the numerical model.

Parameter	Value
Number of blade elements	38
Azimuthal step	$5°$
Aerofoil data	NACA0018 for $Re = 10^6$
Dynamic stall model	None

4. Validation

Comparisons of normalized axial velocity against spanwise distance from the rotor equator is shown in Figures 7 and 8. The operating tip speed ratio is $\lambda = 3.8$ (where the equatorial radius is taken as the reference length dimension) with a wind speed of $U_\infty = 5.5m/s$ and a rotational speed of $\Omega = 1000 RPM$. The comparison shown here are for the extended turbine as shown in Figure 1 since no experimental data is available for the flexed condition. The measurements are shown at two downstream positions of 0.31m and 0.34m (shown in Figure 5). The measurements shown are for a blade azimuth position of $0°$ as shown in Figure 4. For all downstream positions there is clear disagreement particularly at the equator where the experimental result shows a relatively uniform velocity while the numerical model shows a sharp dip. The reason for this can be attributed to the lack of physical accuracy of the lifting line model particularly due to the inaccuracies in 2D aerofoil data (no dynamic stall modelling included) at the low Reynold's number corresponding to this case. Clearly, the observed effect from the numerical model can be attributed to a strong trailing vorticity resulting due to the blade curvature. Some discrepancies may also be observed in the tip region of the blade. Tunnel blockage is also a cause for the observed discrepancies. The effect of blockage is to accelerate the flow past the turbine. This can be particularly observed for $2y/H > 1$ in Figure 7.
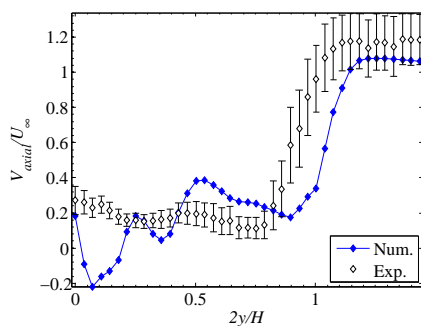

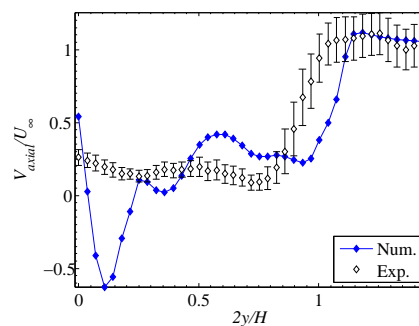**Figure 7.** Axial velocity at x = 0.31m.

Figure 8. Axial velocity at x = 0.34m.

A comparison of the aerodynamic power coefficient for various tip speed ratios between the numerical model and experiment is shown in Figure 9. The numerical model clearly over-predicts the output power. These discrepancies are clearly indicative of the influence of having a relatively low Reynolds number where viscous effects predominate. The vortex model is an inviscid model and hence the over estimation of power is understandable.

5. Results and discussion

The full scale SATVAWT model is now considered by means of a numerical simulation for the extended and flexed conditions as shown in Figure 1 and 2 respectively. All calculations are
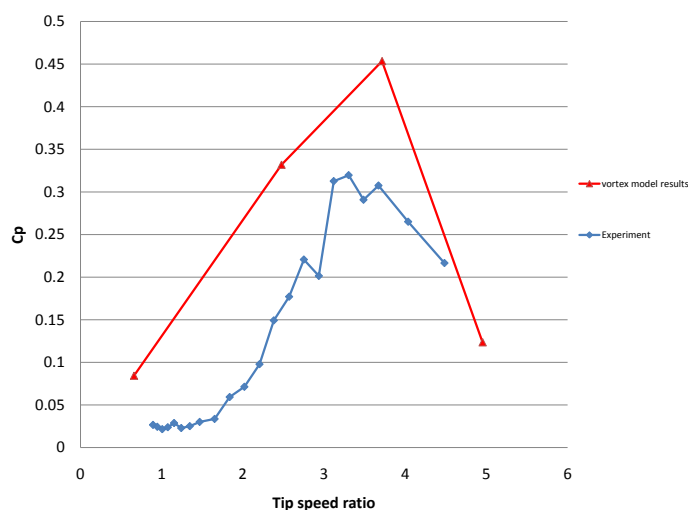
Figure 9. Comparison of power coefficient between the numerical model and the experiment.

performed at the optimal tip speed ratio of 3.8 giving maximum power coefficient.

5.1. Vorticity influence of flexed blades

The bound vorticity variation on the SATVAWT blade gives substantial information on how the blade is aerodynamically loaded during its rotation. Figures 10 and 11 show contour plots of the normalized (with equatorial radius) local blade position s in curvilinear coordinates against azimuthal position for both the extended and flexed conditions respectively. It is clear that for the extended case, for $0° \leq \theta \leq 180°$, the maximum bound vorticity occurs at the equator but is distributed evenly over a large fraction of the blade span. For the flexed blade, the peak bound vorticity increases but is more concentrated at the equator region. The bound vorticity reverses direction for both extended and flexed conditions for $180° \leq \theta \leq 360°$. The magnitude does not reach substantial quantities as for $0° \leq \theta \leq 180°$.

The trailing vorticity variation with azimuth is shown in Figure 12 and 13 for the extended and flexed conditions respectively. As can be observed, the trailing vorticity released in the wake is more intense in the equator region for the flexed blade. Some strong trailing vorticity can also be observed close to the tip where the blade also has curvature. For $180° \leq \theta \leq 360°$, The released trailing vorticity becomes less uniform. The flexed blade again shows stronger vortices in the equatorial region.

The shed vorticity contours shown in Figure 14 and 15 for the extended and flexed conditions respectively do not differ much for azimuth angles $0° \leq \theta \leq 180°$. During the downwind motion of the blade however, the flexed blade shows a more pronounced shed vorticity at the equator.

5.2. Flow field characteristics

The effects of the wake vorticity on the axial velocity component are depicted in Figures 16 and 17 for the extended and flexed conditions respectively. The induction velocity is normalized with the freestream. As can be observed, the wake induction is more uniformly distributed for the extended condition compared to the flexed condition. Although these results show that flexed blades result in a more complex flow field, it is not yet clear how this affects the average power generated.
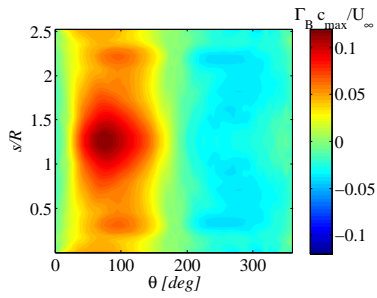
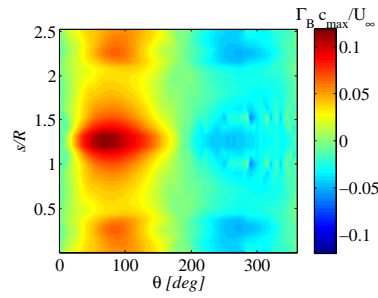**Figure 10.** Bound vorticity: extended turbine ($\lambda = 3.8$).

Figure 11. Bound vorticity: flexed turbine ($\lambda = 3.8$).
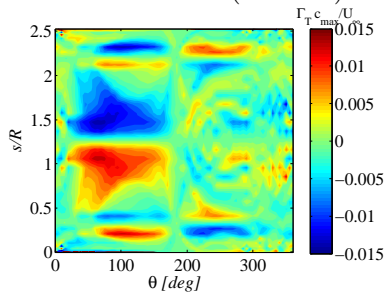

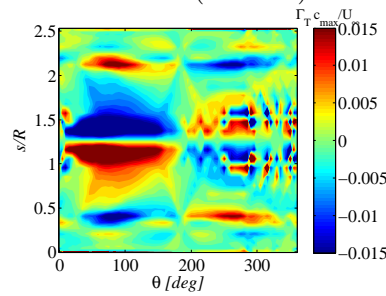**Figure 12.** Trailing vorticity: extended turbine ($\lambda = 3.8$).

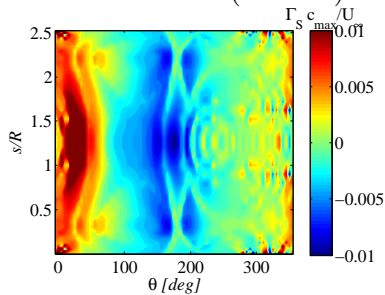**Figure 13.** Trailing vorticity: flexed turbine ($\lambda = 3.8$).

Figure 14. Shed vorticity: extended turbine ($\lambda = 3.8$).
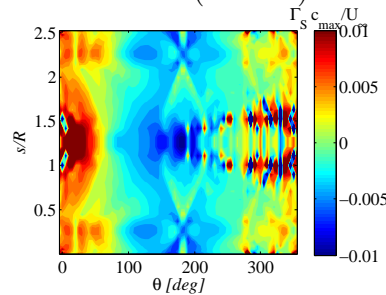

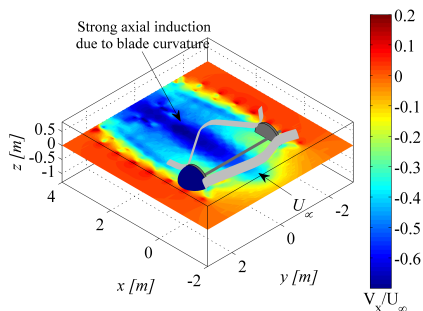**Figure 15.** Shed vorticity: flexed turbine ($\lambda = 3.8$).

Figure 16. Axial wake induced velocities for the extended blade($\lambda = 3.8$).
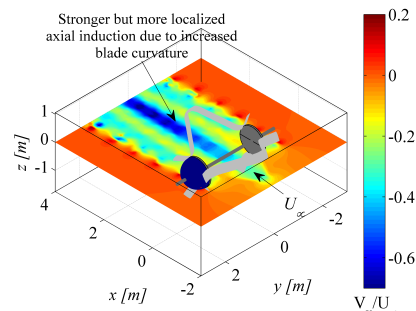

Figure 17. Axial wake induced velocities for the flexed blade ($\lambda = 3.8$).

5.3. Power coefficient

The flow field observations of the previous sections result in different power performance between the extended and flexed conditions. Power coefficient against tip speed ratio is shown in Figure 18. The power coefficient is defined as $C_P = \frac{\bar{P}}{\frac{1}{2}\rho U_\infty^3 A}$ where $\bar{P}$ is the azimuthally averaged power output, U_∞ is the wind speed and A is the turbine projected area.

As can be seen, the flexed turbine geometry gives a lower averaged power coefficient with increasing tip speed ratio. The flexed turbine gives a peak power coefficient which is 13% less than the extended blade configuration. Clearly the concentrated trailing and shed vorticity discussed earlier is one of the causes of this. The effects of self-induced velocities due to the blade curvature still needs to be investigated.
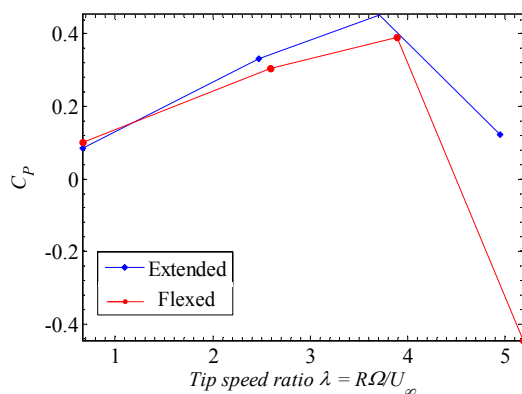

Figure 18. Power coefficient against tip speed ratio for the extended and flexed conditions.

5.4. Blade self-induced velocities

The bound vorticity of a theoretically infinite straight blade is entirely spanwise in direction. This means that each blade section will not be influenced by the bound vorticity of adjacent sections. On the other hand, for the SATVAWT curved blade case, the bound vorticity at a particular section will induce a flow on an adjacent section. This is shown in Figure 19. In this section, this effect is investigated.
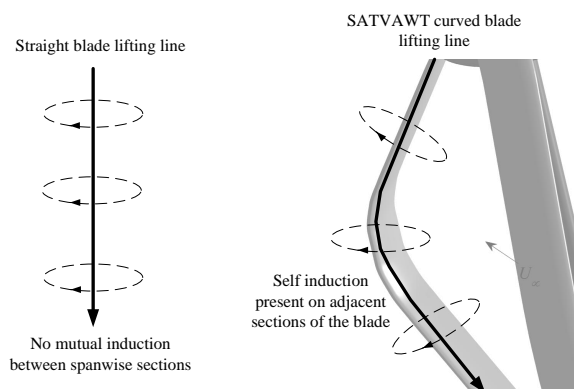

Figure 19. Effect of blade self induction due to curvature. Straight blade case with no self induction due to bound vorticity (left) and SATVAWT curved blade case with self induction due to bound vorticity (right).

Figure 20 shows the total normalized induced axial velocity (V_x) due to the wake and the bound vorticity of the blades, and the component of the axial velocity due to the blade bound vorticities only ($V_{\Gamma,x}$). Both the extended and flexed conditions are shown. The induced velocity is calculated at the lifting line location (quarter-chord blade position). It is clear that the

influence of the blades on the local induction is minimal. A look at the percentage due to bound vorticity to the total induced velocity in Figure 21 shows that for the extended condition the effect of blade vorticity on the axial induced velocity is less than 2% of the total induced velocity.

For the flexed condition, a peak of 7.4% can be observed in the tip vicinity where the blade has a substantial curvature (refer to Figure 2). Another peak reaching 3.8% can also be found close to the equator in the straight part of the blade span between $2 < \frac{s}{R} < 3$. These small percentages suggest that blade curvature does not induce appreciable local axial velocities and hence do not have a major role on the sectional performance of the blade.
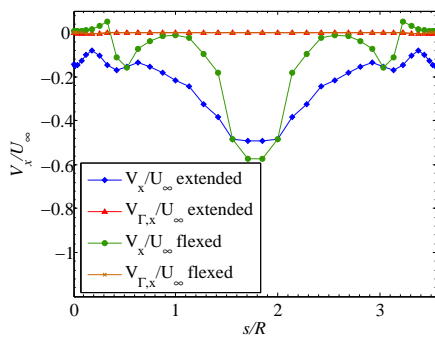

Figure 20. Axial total and blade vorticity induced velocities for the extended and flexed blade configuration ($\lambda = 3.8$).
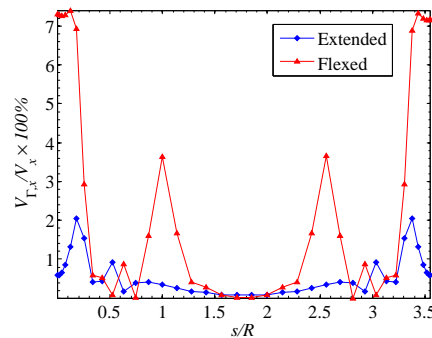
Figure 21. Percentage blade vorticity induced velocities for the extended and flexed blade configuration ($\lambda = 3.8$).

6. Conclusions

Experimental and numerical work has been carried out on a SATVAWT turbine concept. The experimental results were used to validate the numerical results. Some discrepancies were observed and were attributed to limitations in both the experiment as well as the numerical vortex model.

Simulations on the full-scale SATVAWT model highlighted the existence of strong trailing and shed vorticity with increasing blade flexure. This has detrimental effects on performance and is reflected in the power coefficient compared between the extended and flexed turbine conditions. The effect of bound vorticity on the local axial inductions has also been studied but no substantial contribution was observed to the total induced axial velocity.

This study suggests further optimization work in order to find a suitable flexure which can be used without a substantial effect on power performance. Also the dynamic stall phenomenon can be addressed in more detail since this would have particular implications on blade loading and power extraction.

References

[1] C. Hirsch A. F. Abdel Azim El-Sayed and R. Derdelinckx. Dynamics of vertical axis wind turbines (darrieus type). *International Journal of Rotating Machinery*, 2(1):33–41, 1995.

[2] G. van Kuik G. van Bussel C. Ferreira, C. Hofemann. Experimental and numerical investigation of the 3d vawt wake. In *Proceedings of the Euromech Colloquium 508 on wind turbine wakes*, Madrid, Spain, 20-22 October 2009.

[3] Swapnil V. Ghatage and Jyeshtharaj B. Joshi. Optimisation of vertical axis wind turbine: Cfd simulations and experimental measurements. *The Canadian Journal of Chemical Engineering*, 90(5):1186–1201, 2012.

[4] Wouter Haans, Tonio Sant, Gijs van Kuik, and Gerard van Bussel. HAWT near-wake aerodynamics, part I: axial flow conditions. *Wind energ.*, 11(3):19, 2008.

[5] H.H.Bruun. *Hot-Wire Anemometry: Principles and Signal Analysis*. Oxford University Press, USA, 1995.

[6] Mazharul Islam, David S.-K. Ting, and Amir Fartaj. Aerodynamic models for darrieus-type straight-bladed vertical axis wind turbines. *Renewable and Sustainable Energy Reviews*, 12(4):1087 – 1109, 2008.

[7] J. Katz and A. Plotkin. *Low-Speed Aerodynamics*. Cambridge University Press, second edition, 2001.

[8] Matthias Kinzel, Quinn Mulligan, and John O. Dabiri. Energy exchange in an array of vertical-axis wind turbines. *Journal of Turbulence*, 14(6):38–39, 2013.

[9] Frank Scheurich and Richard E. Brown. Modelling the aerodynamics of vertical-axis wind turbines in unsteady wind conditions. *Wind Energy*, 16(1):91–107, 2013.

[10] Carlos Simo Ferreira, Gijs van Kuik, Gerard van Bussel, and Fulvio Scarano. Visualization by piv of dynamic stall on a vertical axis wind turbine. *Experiments in Fluids*, 46:97–108, 2009. 10.1007/s00348-008-0543-z.

[11] A. van Garrel. Development of a wind turbine aerodynamics simulation module. In *ECN-C–03-079*, August 2003.